Electronic Supporting Information (ESI)

Solar cells sensitized by donor-linked concerted companion dyes

Jiaxin Luo,[a] Yuqing Wang,[a] Shaojin Shi,[a] Yuankun Wu,[a] Taochun Ma,[a] Leyao Wang,[a] Glib Baryshnikov,[b] Xinyan Wu,*[a] Chengjie Li*[a] and Yongshu Xie*[a]

[a] Key Laboratory for Advanced Materials and Joint International Research Laboratory of Precision Chemistry and Molecular Engineering, Feringa Nobel Prize Scientist Joint Research Center, Frontiers Science Center for Materiobiology and Dynamic Chemistry, Institute of Fine Chemicals, School of Chemistry and Molecular Engineering, East China University of Science & Technology, Shanghai 200237, China

[b] Department of Science and Technology, Laboratory of Organic Electronics, Linköping University, Norrköping 60174, Sweden

*Email: yshxie@ecust.edu.cn; chengjie.li@ecust.edu.cn; xinyanwu@ecust.edu.cn.

Contents

1 Experimental section

1.1 Materials and instrumentation

All chemical reagents and solvents of analytical grade were purchased and used without further purification unless otherwise noted. Fluorine-doped SnO_2 conducting glass (FTO glass, transparency > 90% in the visible range, sheet resistance 15 Ω/square) was purchased from the Advanced Election Technology Co., Ltd. TiO_2 paste (18 NR-T and 18 NR-AO) was purchased from the Greatcell Solar Industries Pty Ltd.

^{1}H NMR and ^{13}C NMR spectra were recorded using a Bruker AM 400 spectrometer at 298 K with tetramethylsilane (TMS) used as the internal standard. HRMS data were collected using a Waters LCT Premier XE spectrometer or a JEOL-JMS-T100LP AccuTOF spectrometer. Matrix-assisted laser desorption/ionization time-of-flight mass spectra (MALDI-TOF-MS) were measured on a Shimadzu-Kratos model Axima CFR + mass spectrometer using dithranol as the matrix. UV-Vis absorption spectra were measured on a Shimadzu UV2600 spectrophotometer, and fluorescence spectra were recorded on a Varian Cary Eclipse fluorescence spectrophotometer. The cyclic voltammograms of the dyes were carried out in CH_2Cl_2 on a CorrTest electrochemical workstation based on a three electrode system using 0.1 M $TBAPF_6$ in CH_2Cl_2 as the supporting electrolyte, a platinum ring as the working electrode, a platinum wire as the counter electrode, and a Ag/AgCl electrode in saturated KCl solution as the reference electrode. The scan rate was fixed at 100 mV s^{-1}.

Photovoltaic measurements were performed by employing an AM 1.5 solar simulator equipped with a 300 W xenon lamp (model No. 91160, Oriel). The power of the simulated light was calibrated to 100 mW cm^{-2} using a Newport Oriel PV reference cell system (model 91150 V). *J–V* curves were obtained by applying an external bias to the cell and measuring the generated photocurrent with a model 2400 source meter (Keithley Instruments, Inc. USA). The voltage step and delay time of the photocurrent were 10 mV and 40 ms, respectively. Action spectra of the incident monochromatic photon-to-electron conversion efficiency (IPCE) for the solar cells were obtained with a Newport-74125 system (Newport Instruments). The intensity of monochromatic light was measured with a Si detector (Newport 71640). The electrochemical impedance spectroscopy (EIS) measurements of all the DSSCs were performed using a Zahner IM6e Impedance Analyzer (ZAHNER-Elektrik GmbH & CoKG, Kronach, Germany), with the frequency range of 0.1 Hz–100 kHz and the alternative signal of 10 mV. The ZSimpWin software was used to fit the experimental EIS data.

1.2 Fabrication of the solar cells

The FTO conducting glass was washed with a detergent solution, deionized water, acetone and ethanol successively for 20 min under ultrasonication before use. For cobalt-based electrolyte, the FTO glass plates were immersed in 40 mM $TiCl_4$ aqueous solution at 70 °C for 30 min, then washed with deionized water and ethanol. The pretreated FTO glass was heated at 450 °C for 30 min. The TiO_2 photoanode was then prepared by repetitive screen-printing. Afterwards, the TiO_2 films were heated with a programmed procedure at 275 °C for 5 min, 325 °C for 5 min, 375 °C for 5 min, 450 °C for 15 min, and 500 °C for 15 min. The resulting layers were post-treated with 40 mM $TiCl_4$ aqueous solution at 70 °C for 30 min and sintered once again at 450 °C for 30 min. The active area of the TiO_2 photoanode is 0.12 cm^2. Then they were immersed in a 0.2 mM solution of the porphyrin dyes or CC dyes or a 0.3 mM solution of the organic dyes in a mixture of chloroform and ethanol (volume ratio of 1:1) for 10 h at 25 °C for dye uptake. For the counter electrode, H_2PtCl_6 in 2-propanol was evenly distributed on FTO glass through spin coating, and the cathode was heated at 400 °C for 15 min. Eventually, the two electrodes were sealed with thermoplastic Surlyn (25 μm), and the electrolyte solution was injected through a hole in the counter electrode to complete the fabrication of the sandwich-type solar cells. The iodine-based electrolyte was composed of 0.1 M LiI, 0.05 M I_2, 0.6 M 1, 2-dimethyl-3-propyl-imidazolium iodide (DMPII) and 0.5 M 4-tert-butylpyridine (TBP) in acetonitrile. The cobalt-based electrolyte was composed of 0.22 M $[Co(bpy)_3](TFSI)_2$, 0.05 M $[Co(bpy)_3](TFSI)_3$, 0.1 M LiTFSI, and 0.6 M TBP in acetonitrile.

1.3 Theoretical calculation details

Theoretical calculations were carried out using Gaussian16 program package at basis set of ZDO and method of PM6.[1, 2]

2 Absorption data and emission spectra

Table S1 Absorption data for the sensitizers.

Dyes	λ_{max}[a]/ nm (ε / 10^3 $M^{-1}cm^{-1}$)	λ_{max}[b]/ nm
XW85	456 (338.2), 664 (69.1)	656
XW86	456 (332.6), 664 (68.0)	656
XL3	365 (42.2), 507 (32.7)	512
XW10	457 (342.7), 590 (12.1), 664 (84.9)	663
XW76	360 (69.0), 458 (342.0), 664 (75.8)	658

a) Absorption maxima of the sensitizers in THF; b) absorption maxima of the sensitizers adsorbed on TiO_2 films (2 μm).

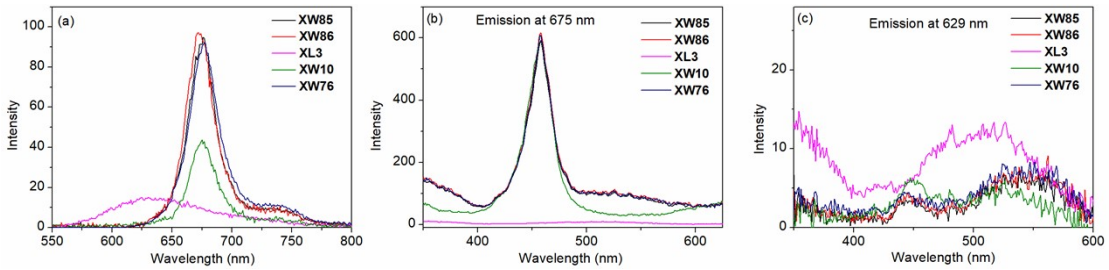

Figure S1 Fluorescence spectra of the dyes in THF (1×10^{-6} M). Emission spectra, λ_{ex} = 507 nm (a); and excitation spectra, λ_{em} = 675 nm (b), and λ_{em} = 629 nm (c).

3 Electrochemical behavior

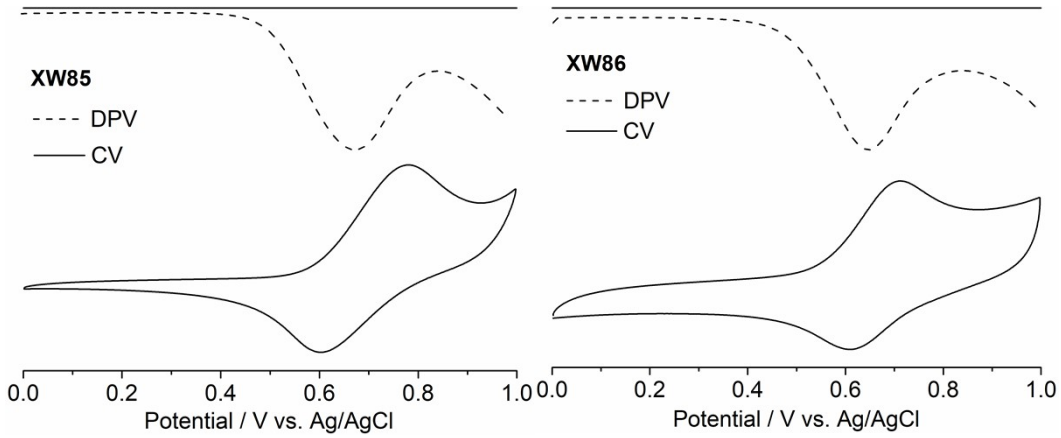

Figure S2 Cyclic voltammetry (CV) and differential pulse voltammetry (DPV) plots of **XW85** and **XW86** versus Ag/AgCl electrode.

4 Photovoltaic properties

Table S2 Photovoltaic parameters for the DSSCs based on the sequential cosensitization of **XW10** and **XL3**.

Devices	V_{OC} / mV	J_{SC} / mA·cm^{-2}	FF / %	PCE / %	Dye loading [×10^{-7} mol·cm^{-2}]	
					XW10	**XL3**
S1[a]	779	17.02	69.56	9.22	0.25	1.70
	782	17.30	69.42	9.39		
	778	16.92	69.99	9.22		
	776	16.97	69.94	9.21		
Averaged values	779±2	17.05±0.15	69.73±0.24	9.26±0.08		
S2[b]	782	16.85	69.37	9.14	0.21	1.83
	780	17.11	68.76	9.17		
	786	17.15	69.43	9.36		
	786	16.58	68.86	8.98		
Averaged values	783±3	16.92±0.23	69.11±0.30	9.16±0.14		
S3[c]	783	16.68	69.21	9.04	0.16	1.98
	790	16.50	69.73	9.09		
	792	16.60	69.26	9.10		
	788	16.73	69.00	9.09		
Averaged values	788±3	16.63±0.09	69.3±0.27	9.08±0.02		

Sensitization time: a) **XW10** (10 h), **XL3** (1.5 h); b) **XW10** (10 h), **XL3** (2.5 h); c) **XW10** (10 h), **XL3** (3.5 h).

Table S3 Photovoltaic parameters for the DSSCs based on the cocktail cosensitization of **XW10** and **XL3** (sensitization time: 10 h).

Devices	V_{OC} / mV	J_{SC} / mA·cm^{-2}	FF / %	PCE / %	Dye loading [×10^{-7} mol·cm^{-2}]	
					XW10	**XL3**
M1[a]	775	16.69	69.88	9.04	0.083	2.18
	780	16.20	69.63	8.80		
	784	15.85	69.85	8.68		
	782	16.14	70.85	8.94		
Averaged values	780±3	16.22±0.30	70.05±0.47	8.87±0.14		
M2[b]	787	15.94	70.46	8.83	0.070	2.31
	781	16.28	70.00	8.89		
	780	16.71	70.80	9.23		
	787	16.64	71.13	9.31		
Averaged values	784±3	16.39±0.31	70.6±0.42	9.07±0.21		
M3[c]	791	16.23	70.63	9.06	0.042	2.35
	789	16.64	70.62	9.27		
	797	16.95	70.20	9.49		
	799	16.57	70.14	9.28		
Averaged values	794±4	16.6±0.26	70.4±0.23	9.28±0.15		

Concentrations: a) **XW10** (0.2 mM), **XL3** (0.1 mM); b) **XW10** (0.15 mM), **XL3** (0.15 mM); c) **XW10** (0.1 mM), **XL3** (0.2 mM).

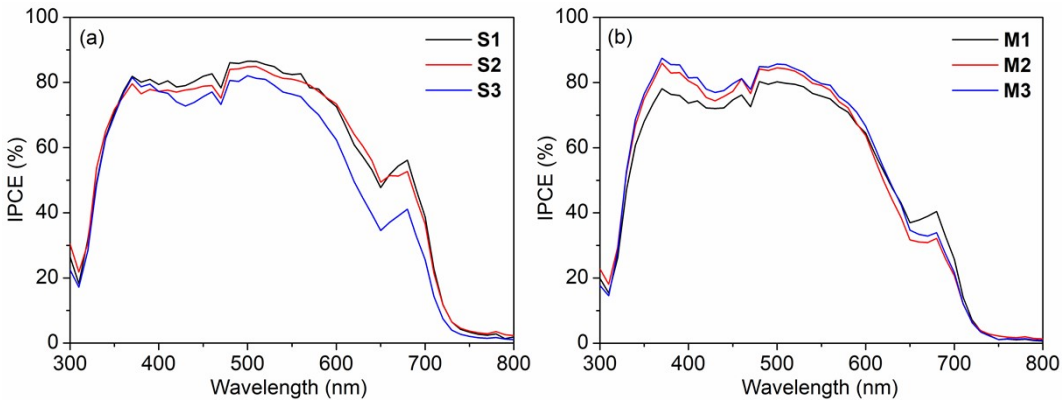

Figure S3 IPCE spectra of the DSSCs based on a) sequential and b) cocktail cosensitization.

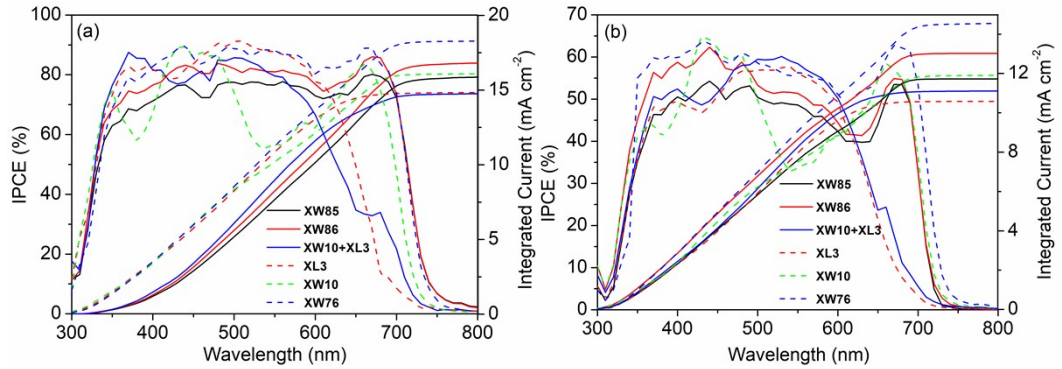

Figure S4 IPCE spectra and integral J_{SC} curves for the DSSCs based on (a) I_3^-/I^- and (b) $Co^{3+/2+}$ electrolytes.

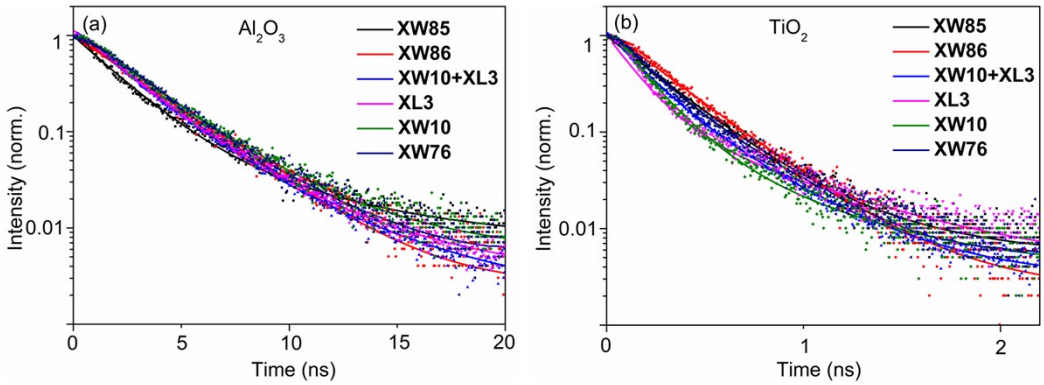

Figure S5 PL decay traces of dye-grafted (a) Al_2O_3 films and (b) TiO_2 films. Excitation wavelength: 450 nm. Emission wavelength: 680 nm for **XW85**, **XW86**, **XW10**, **XW76**; 630 nm for **XW10**+**XL3**, **XL3**.

Table S4 Time coefficients and relative amplitudes of PL decay traces.

Dyes	Film	τ_1 (ns)	A_1 (%)	τ_2 (ns)	A_2 (%)	τ_{av} [a](ns)	η_{inj} [b](%)
XW85	Al_2O_3	0.84	55.36	3.35	44.64	1.96	85.81
	TiO_2	0.16	79.35	0.72	20.65	0.28	
XW86	Al_2O_3	1.16	44.80	2.78	55.20	2.05	86.13
	TiO_2	0.14	73.85	0.69	26.15	0.29	
XW10+**XL3**	Al_2O_3	1.05	32.27	2.61	67.73	2.11	88.01
	TiO_2	0.13	77.53	0.67	22.47	0.25	
XL3	Al_2O_3	0.98	41.19	2.97	58.81	2.15	89.56
	TiO_2	0.12	86.53	0.90	13.47	0.23	
XW10	Al_2O_3	1.06	44.00	3.14	56.00	2.23	88.33
	TiO_2	0.11	79.47	0.84	20.53	0.26	
XW76	Al_2O_3	1.06	43.91	3.06	56.09	2.18	87.40
	TiO_2	0.14	75.75	0.70	24.25	0.28	

a) The values of τ_{av} were determined with $\tau_{av} = \sum_{i=1}^{n} A_i \tau_i$; b) $\eta_{inj} = 1 - \tau_{TiO_2}/\tau_{Al_2O_3}$.[3]

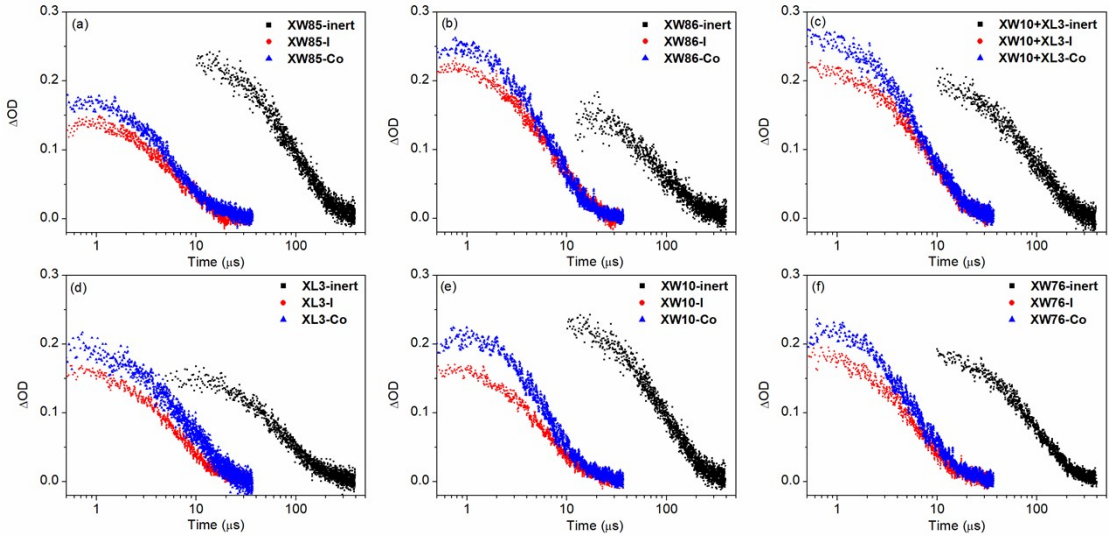

Figure S6 Transient absorption profiles of the TiO_2 films sensitized with (a) **XW85**, (b) **XW86**, (c) **XW10**+**XL3**, (d) **XL3**, (e) **XW10**, and (f) **XW76** with inert electrolyte (0.1 M TBP and 0.1 M LiTFSI in acetonitrile), iodine-based electrolyte, and cobalt-based electrolyte, respectively. Excitation wavelengths: 450 nm for **XW85**, **XW86**, **XW10**, and **XW76**; 532 nm for **XW10**+**XL3** and **XL3**. Probe wavelength: 780 nm. The fitted times are obtained by the multi-exponential function.

Table S5 Recombination time constants (τ_{rec}) and regeneration half times ($\tau_{1/2}$) extracted from transient absoption measurement and the calculated dye regeneration efficiencies ($\eta_{reg}=1-\tau_{electrolyte}/\tau_{inert}$). [3]

Dyes	τ_{rec} (μs)	$\tau_{1/2}$-I (μs)	η_{reg}-I (%)	$\tau_{1/2}$-Co (μs)	η_{reg}-Co (%)
XW85	82	5.7	93.0	6.9	91.6
XW86	79	6.7	91.5	5.6	92.9
XW10+XL3	96	8.4	91.3	8.0	91.2
XL3	99	7.1	92.8	9.3	90.6
XW10	82	5.9	92.8	6.5	92.1
XW76	86	6.3	92.7	5.6	93.5

5 Desorption curves and linear fitting

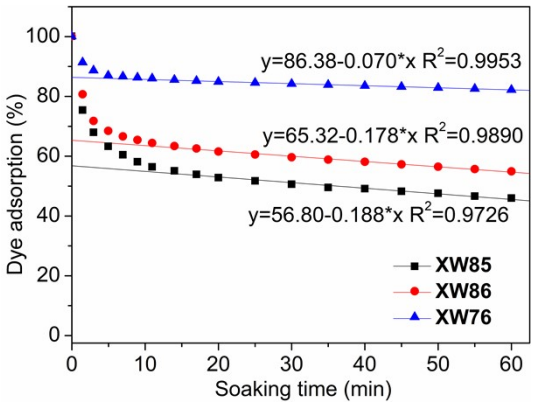

Figure S7 The desorption curves for the dyes and the linear fitting of the slow desorption processes for calculating the double-anchoring dye amounts, and the corresponding data are listed in **Table S6**.

Table S6 The double-anchoring and single-anchoring dye amounts obtained from the linear fitting of the desorption curves.[a]

Samples	double-anchoring (%)	single-anchoring (%)	double/single ratio
XW85	56.80	43.20	1.31
XW86	65.32	34.68	1.88
XW76	86.38	13.62	6.34

a) The proportion of double-anchoring was estimated according to the intercept of the fitting curve, while the remainder was that of single-anchoring.

6 FTIR spectra

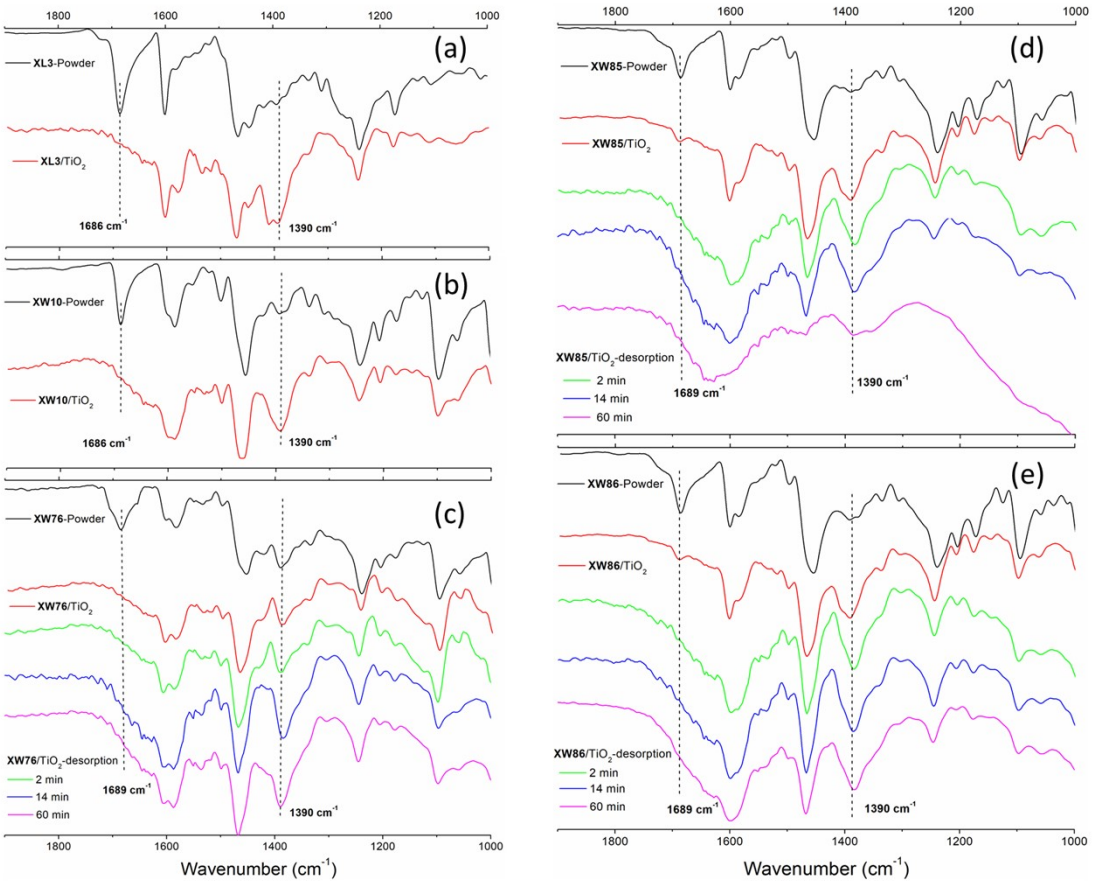

Figure S8 ATR-FTIR spectra of the dyes in the powder state, and adsorbed on the TiO_2 films. For the CC dyes, the IR changes during the desorption processes are shown at time intervals indicated in (c), (d), and (e).

7 Theoretical calculations

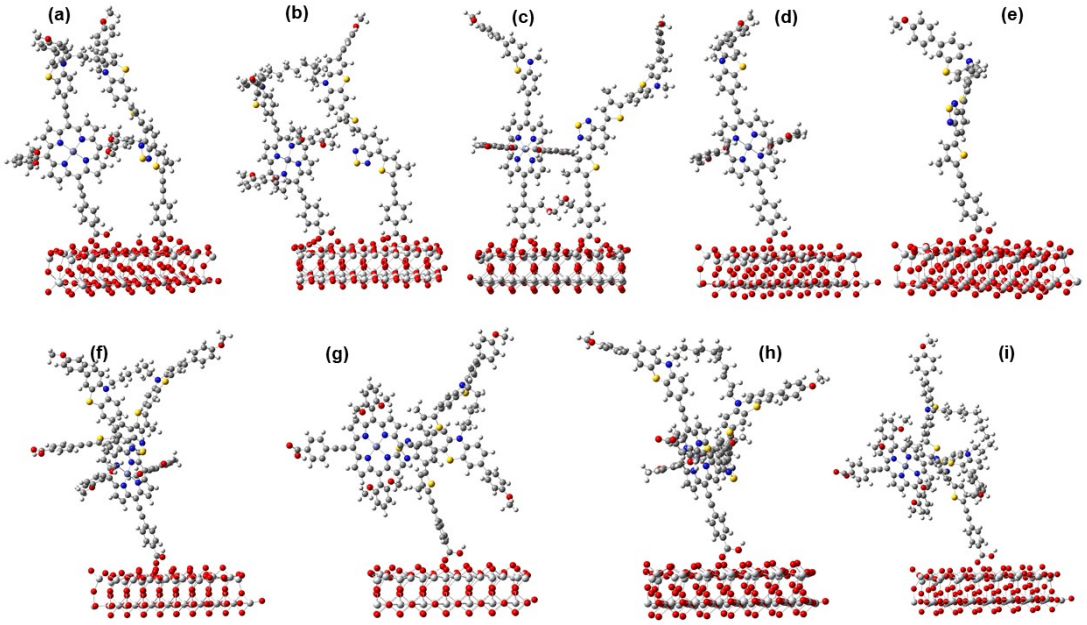

Figure S9 The optimized structures for the dyes adsorbed on the TiO_2 surface for **XW85** (a), **XW86** (b) and **XW76** (c) in double-anchoring mode, and **XW10** (d), **XL3** (e), as well as the single-anchoring modes for **XW85** and **XW86** *via* the porphyrin unit (f, h) and the organic unit (g, i), respectively.

Table S7 The calculated binding energies (E_{be}) for the dyes anchored on TiO_2 in different modes.

Dyes	**XW85**[a]	**XW85**[b]	**XW85**[c]	**XW86**[a]	**XW86**[b]	**XW86**[c]	**XW76**[a]	**XL3**	**XW10**
E_{be} (kcal/mol)	23.8	1.7	8.9	26.0	6.1	11.0	38.4	2.1	2.1

a) Double-anchored dyes; b) single-anchored dyes *via* the organic unit; and (c) single-anchored dyes *via* the porphyrin unit.

8 Electrochemical impedance spectroscopy

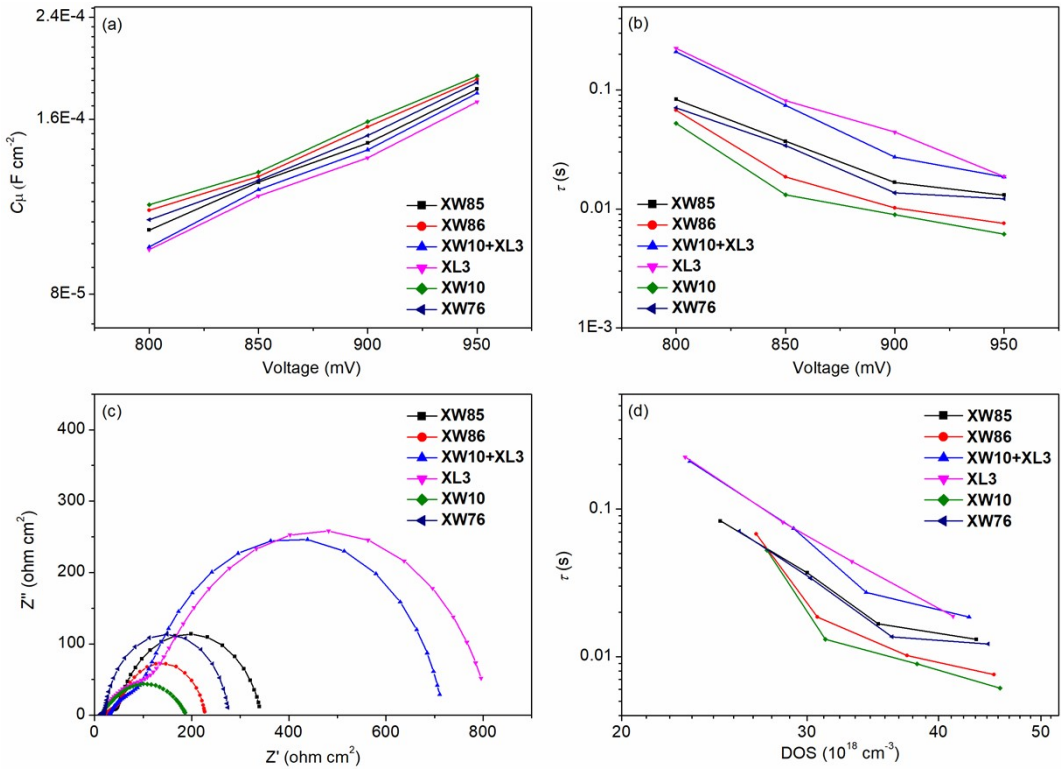

Figure S10 Plots of (a) C_μ, (b) τ versus the bias voltages, (c) complex-plane plots at bias potential of −0.85 V, and (d) τ versus *DOS* of the DSSCs using the $Co^{3+/2+}$ electrolyte.

Table S8 Fitted EIS parameters for all devices using I_3^-/I^- at a bias potential of −0.75 V and $Co^{3+/2+}$ at a bias potential of −0.85 V.[a]

Dyes	Electrolytes	C_μ (mF cm^{-2})	R_{rec} (Ω cm^2)	R_{tr} (Ω cm^2)	τ (s)	η_{col}[b] (%)
XW85	I_3^-/I^-	0.369	199.9	14.2	0.074	93.3
XW86	I_3^-/I^-	0.373	81.8	11.1	0.031	88.1
XW10+XL3	I_3^-/I^-	0.370	698.6	18.3	0.259	97.4
XL3	I_3^-/I^-	0.366	784.1	15.3	0.287	98.1
XW10	I_3^-/I^-	0.368	60.0	9.9	0.022	85.8
XW76	I_3^-/I^-	0.387	171.6	12.9	0.066	93.0
XW85	$Co^{3+/2+}$	0.125	296.1	48.4	0.037	85.9
XW86	$Co^{3+/2+}$	0.127	145.8	28.0	0.019	83.9
XW10+XL3	$Co^{3+/2+}$	0.121	609.5	79.6	0.074	88.4
XL3	$Co^{3+/2+}$	0.118	688.2	111.1	0.081	86.1
XW10	$Co^{3+/2+}$	0.130	101.1	19.5	0.013	83.8
XW76	$Co^{3+/2+}$	0.126	271.0	47.2	0.034	85.2

a) R_{rec}: Charge recombination resistance, R_{tr}: transport resistance, η_{col}: charge collection efficiency; b) $\eta_{col} = (1 + R_{tr} / R_{rec})^{-1}$.[4]

9 Characterization spectra for the compounds

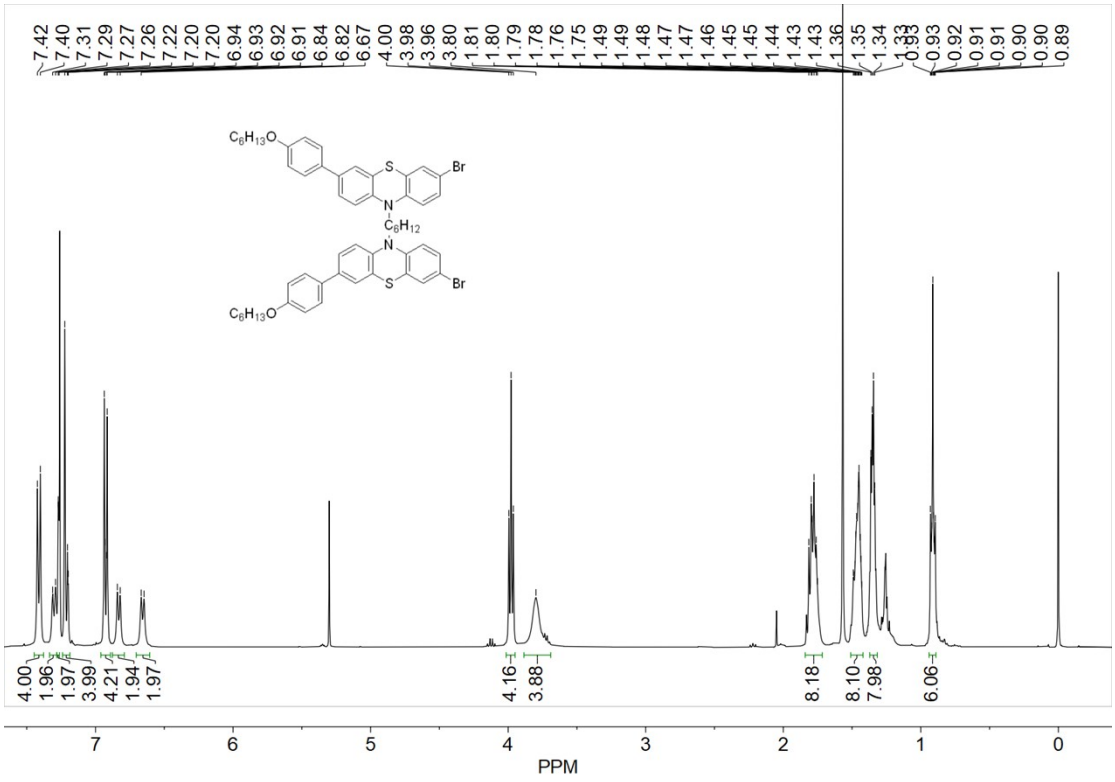

Figure S11 The ^{1}H NMR spectrum of compound **1a** in $CDCl_3$.

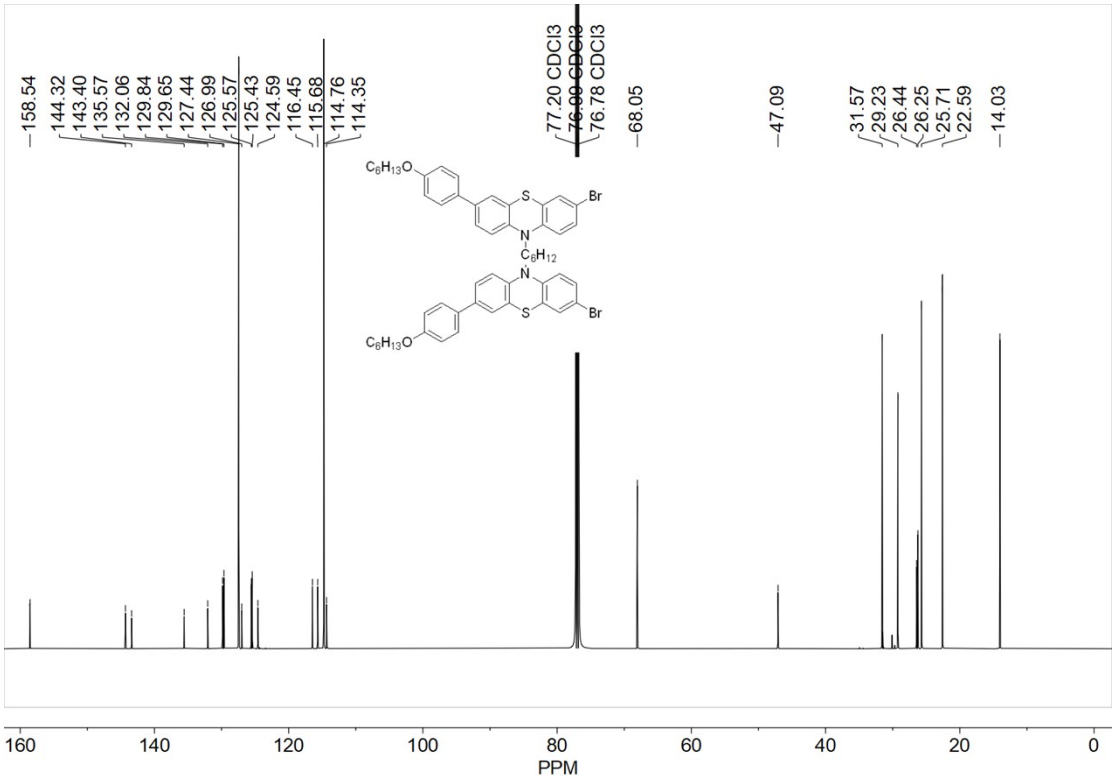

Figure S12 The ^{13}C NMR spectrum of compound **1a** in $CDCl_3$.

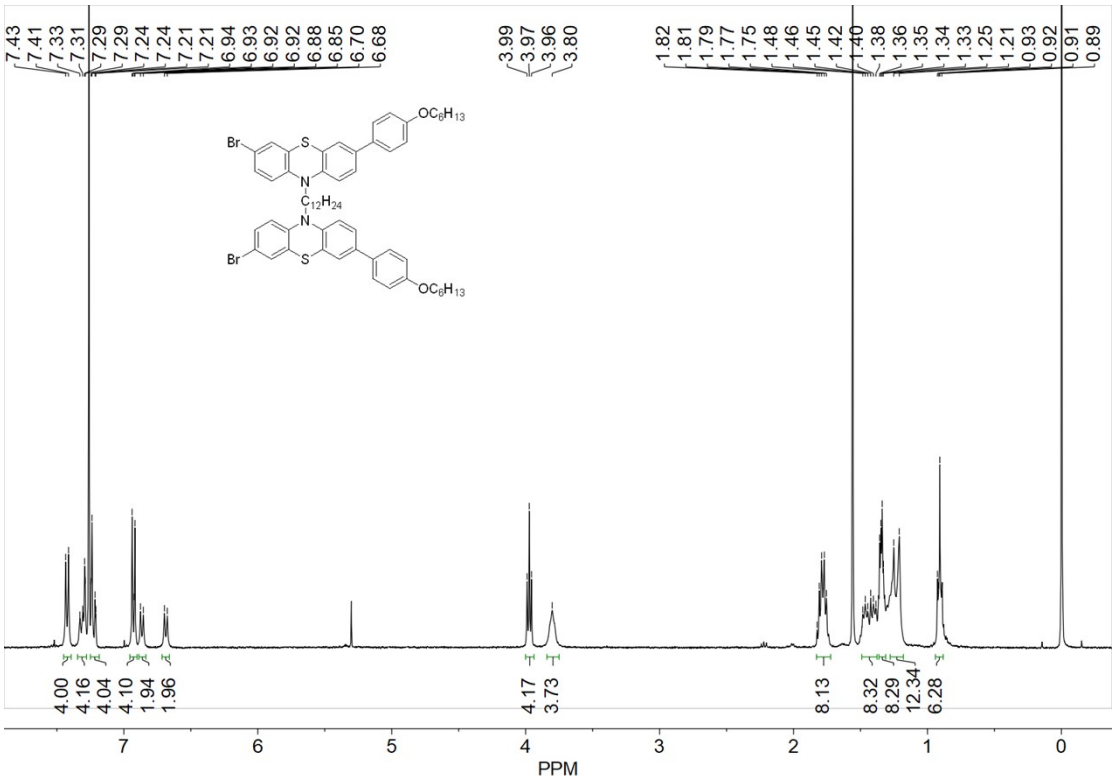

Figure S13 The ^{1}H NMR spectrum of compound **1b** in $CDCl_3$.

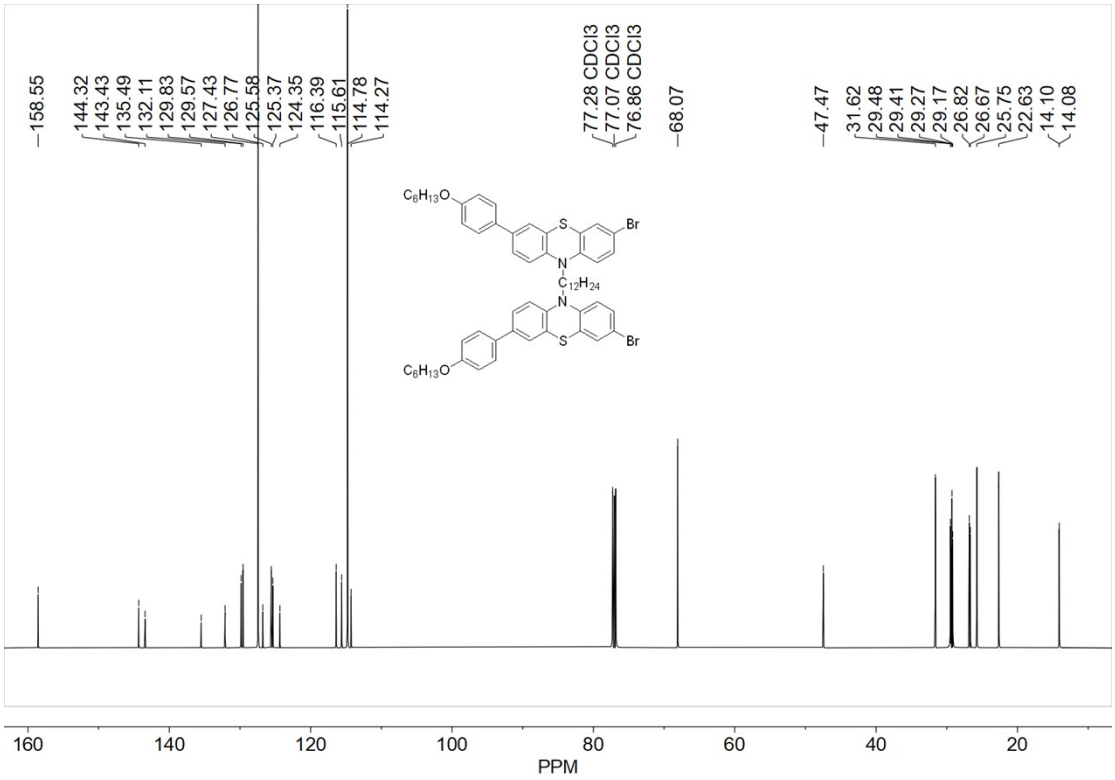

Figure S14 The ^{13}C NMR spectrum of compound **1b** in $CDCl_3$.

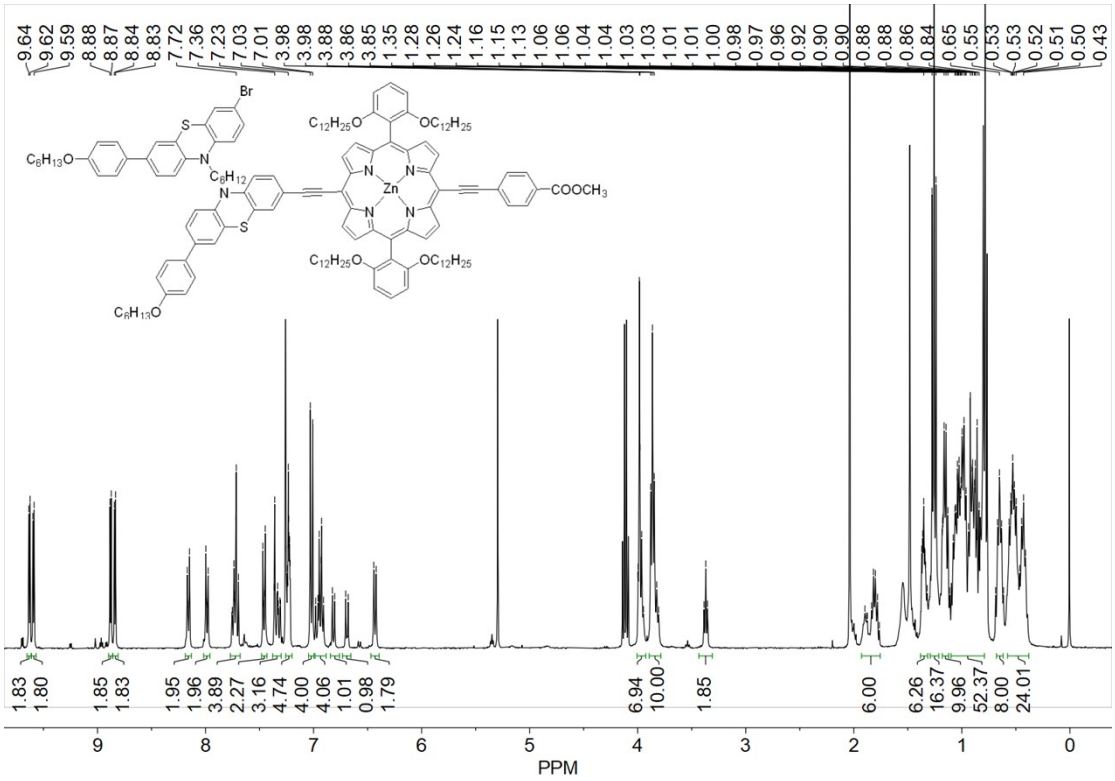

Figure S15 The ^{1}H NMR spectrum of compound **2a** in $CDCl_3$.

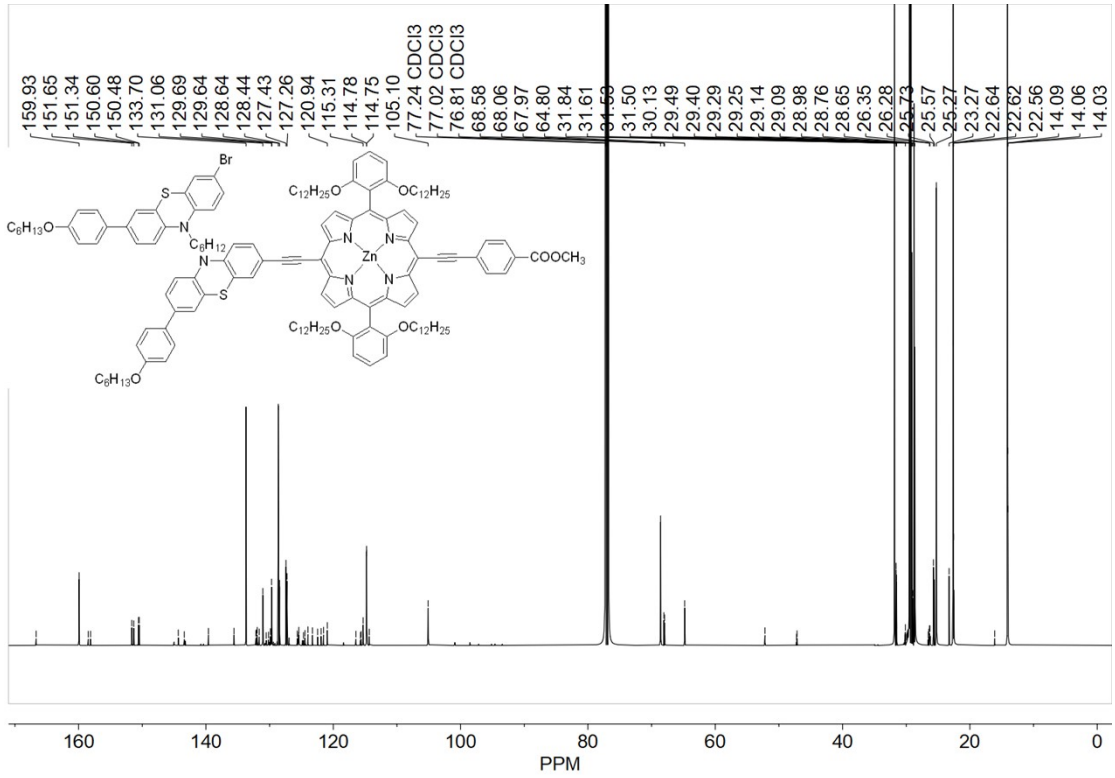

Figure S16 The ^{13}C NMR spectrum of compound **2a** in $CDCl_3$.

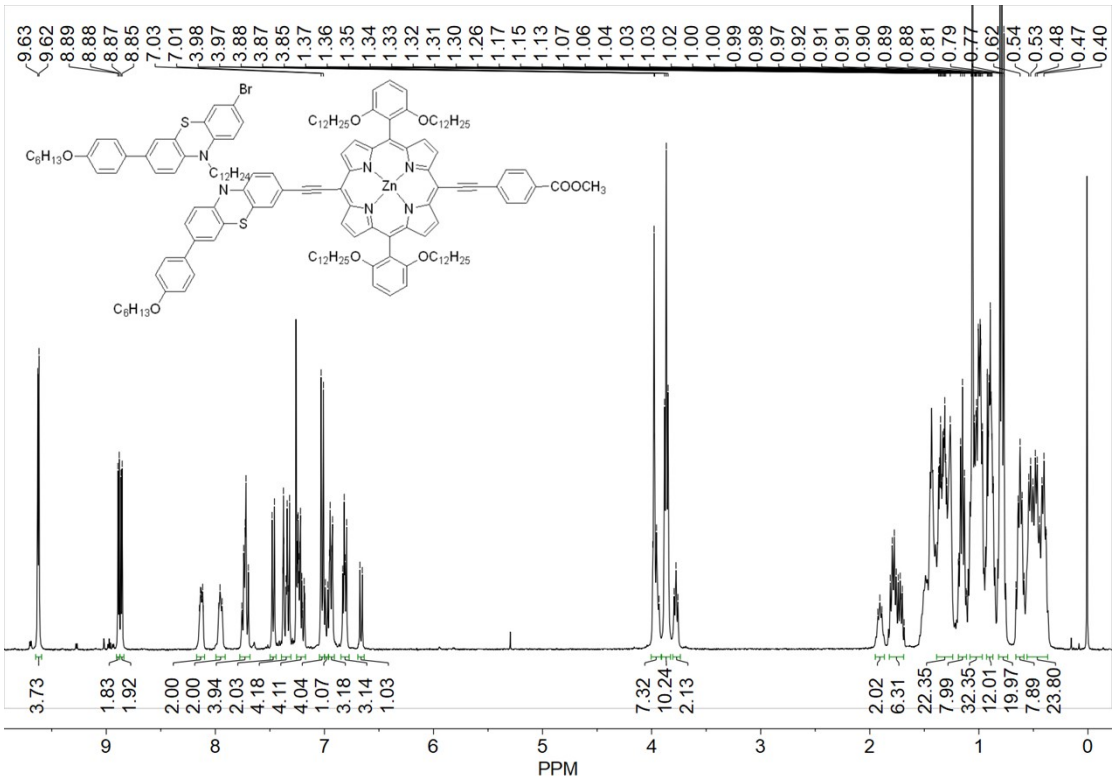

Figure S17 The ^{1}H NMR spectrum of compound **2b** in $CDCl_3$.

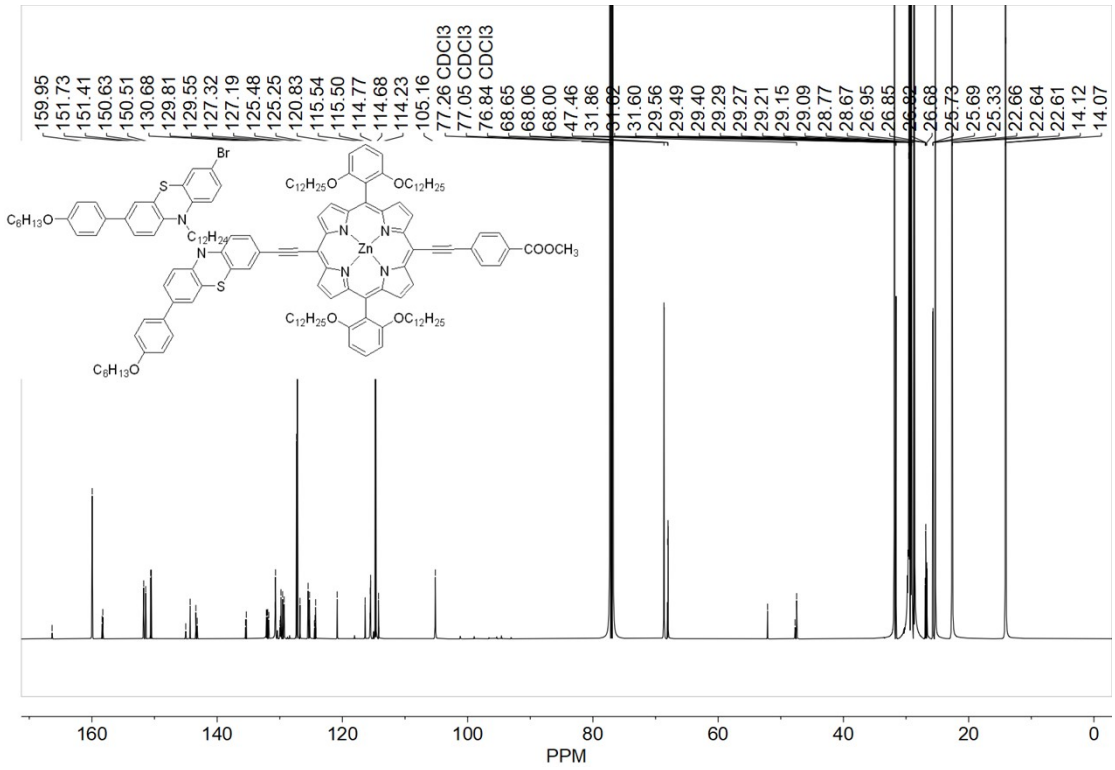

Figure S18 The ^{13}C NMR spectrum of compound **2b** in $CDCl_3$.

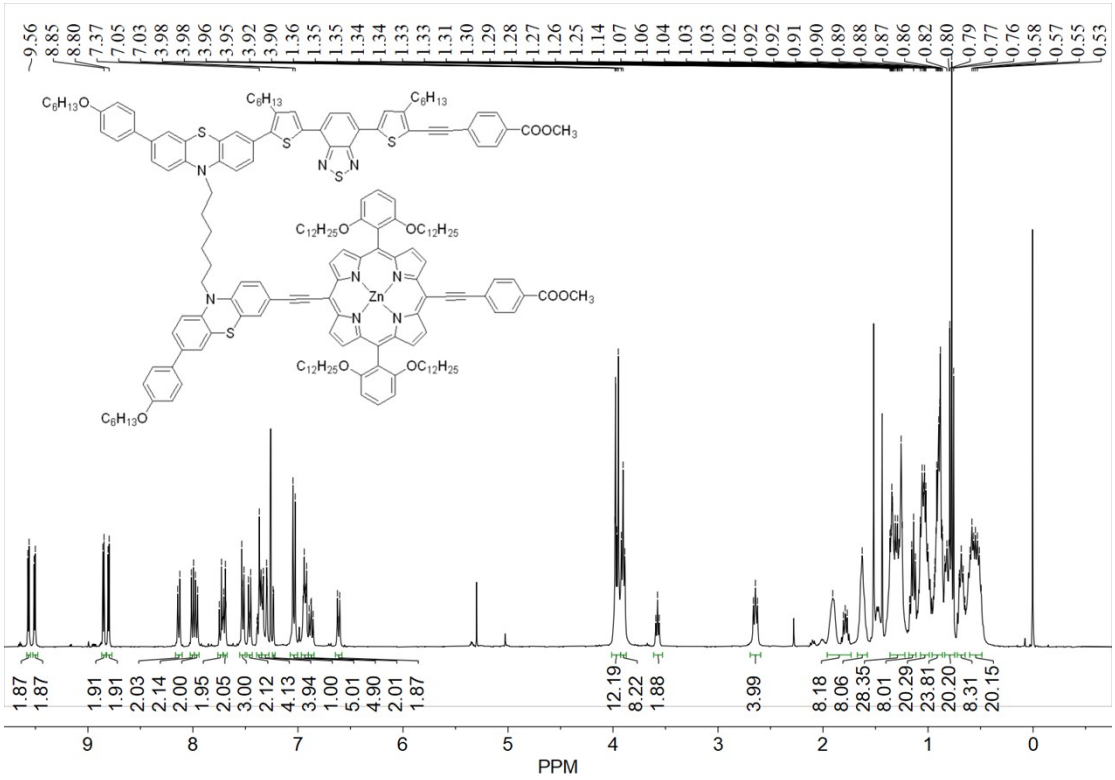

Figure S19 The ^{1}H NMR spectrum of compound **3a** in $CDCl_3$.

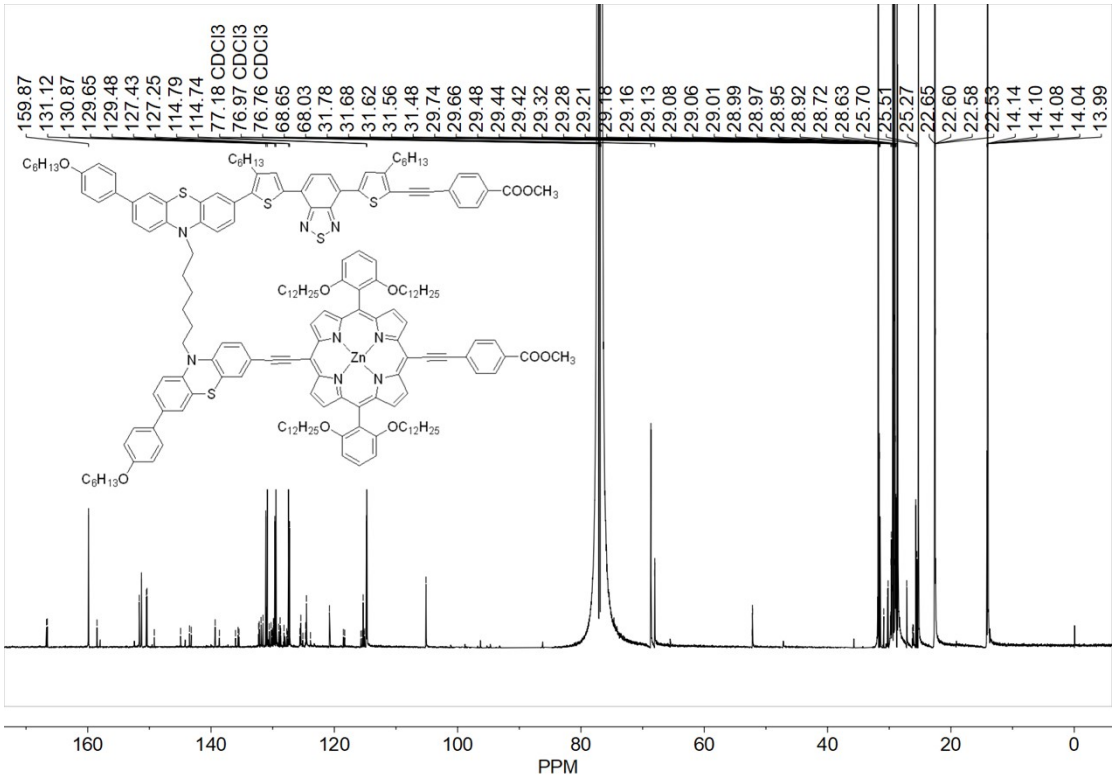

Figure S20 The ^{13}C NMR spectrum of compound **3a** in $CDCl_3$.

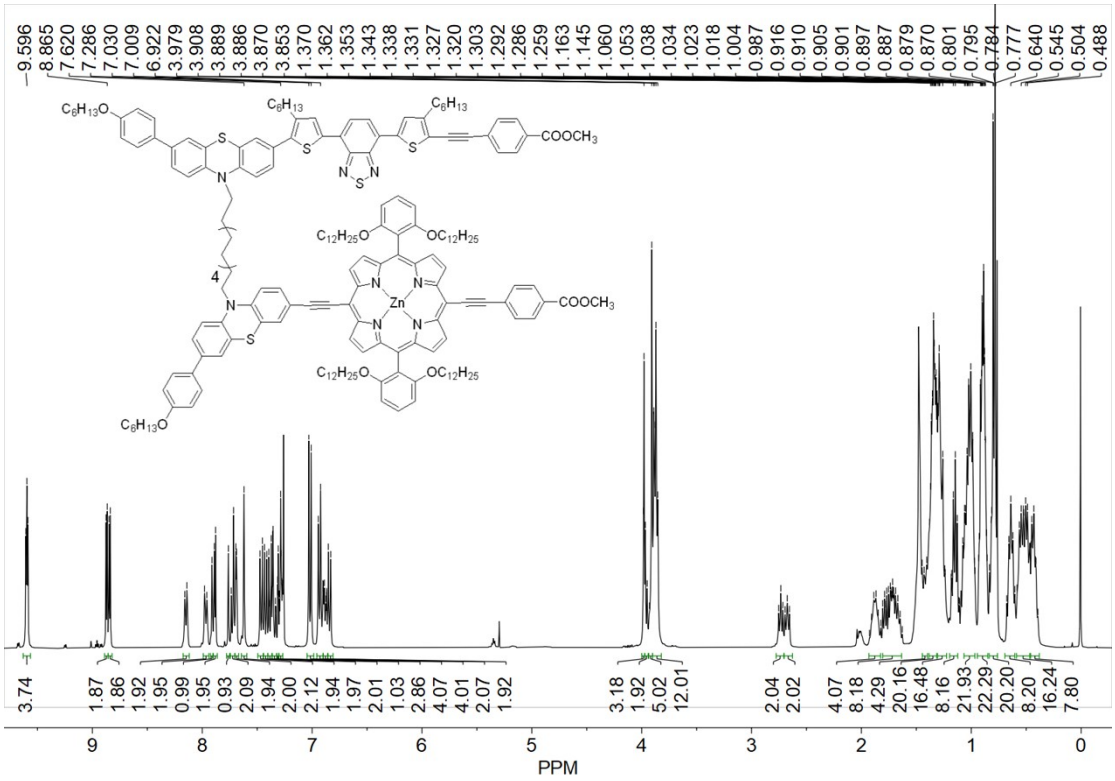

Figure S21 The ^{1}H NMR spectrum of compound **3b** in $CDCl_3$.

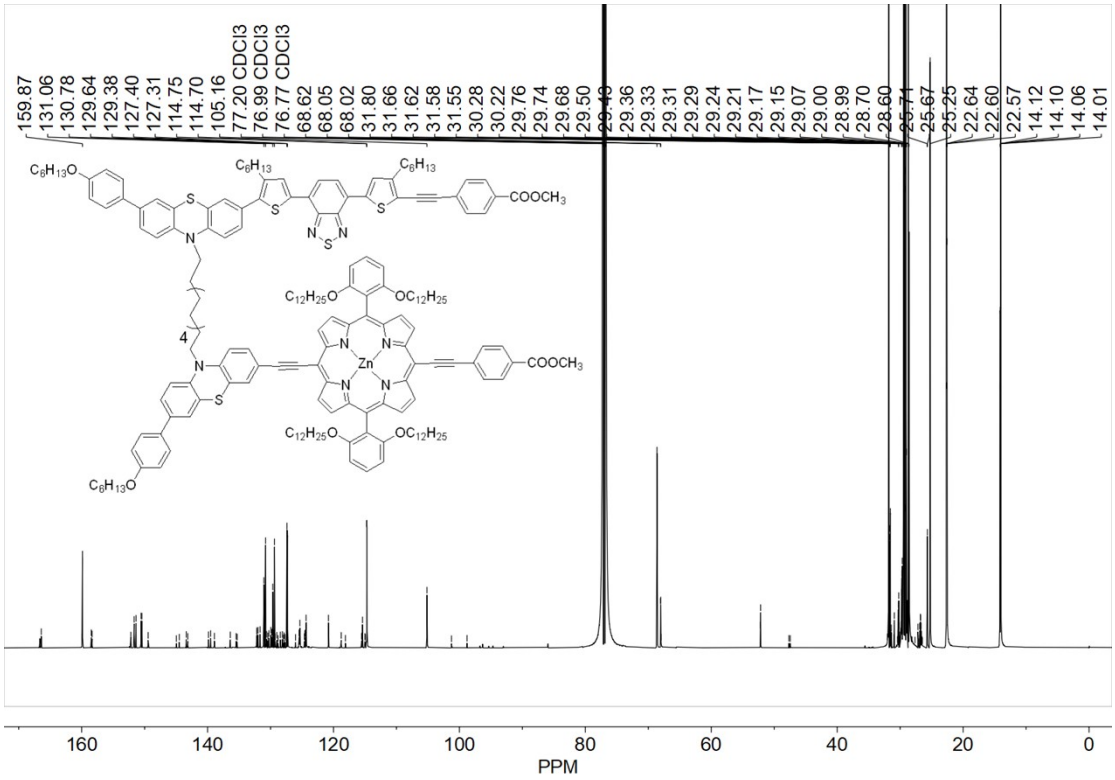

Figure S22 The ^{13}C NMR spectrum of compound **3b** in $CDCl_3$.

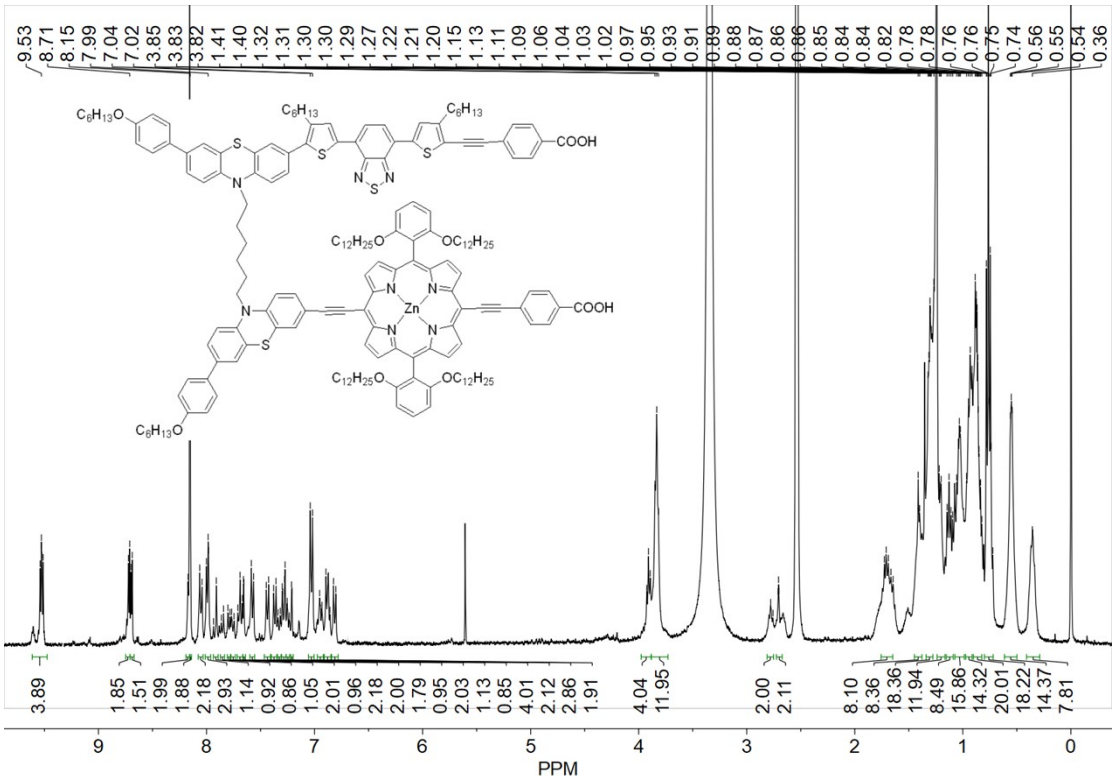

Figure S23 The ^{1}H NMR spectrum of compound **XW85** in $CDCl_3$/DMSO-d_6 (1/2, v/v).

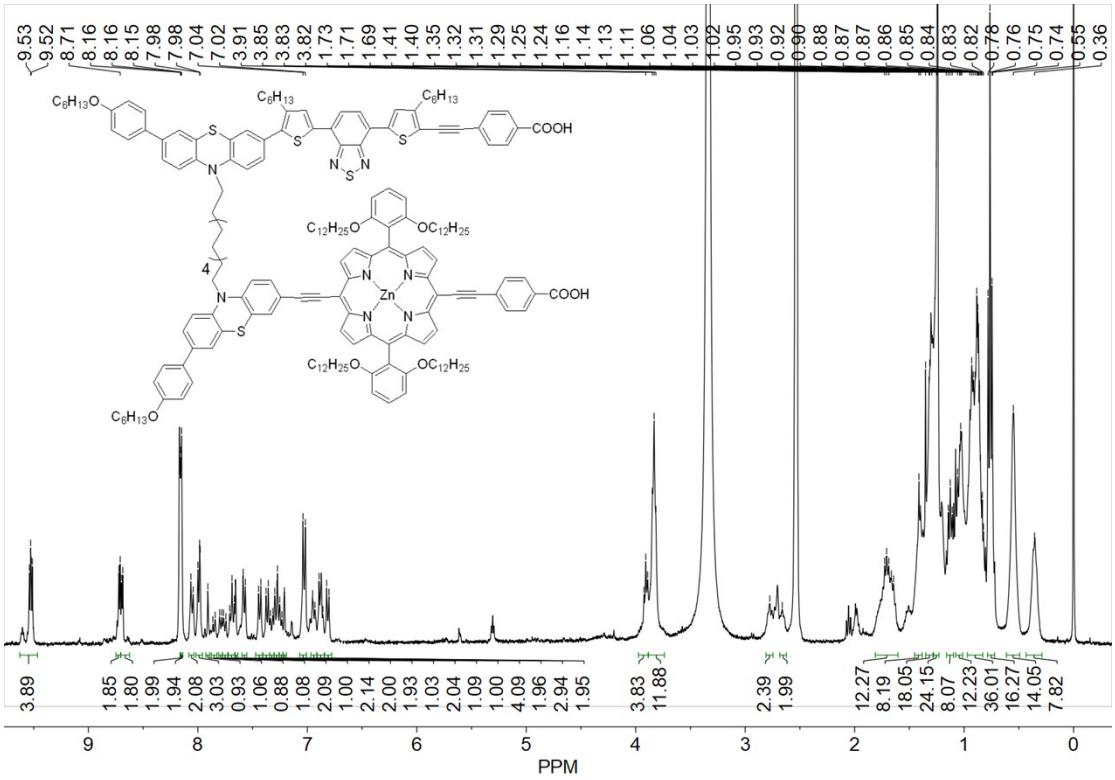

Figure S24 The ^{1}H NMR spectrum of compound **XW86** in $CDCl_3$/DMSO-d_6 (1/2, v/v).

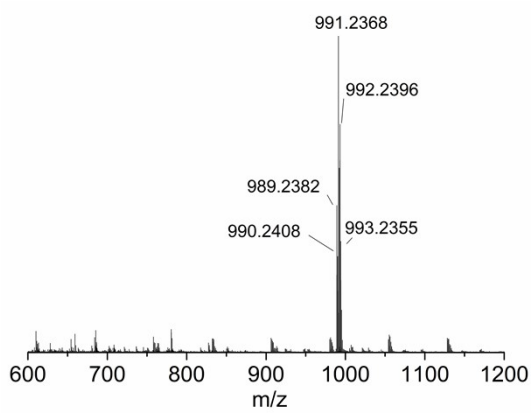

Figure S25 HRMS of compound **1a**.

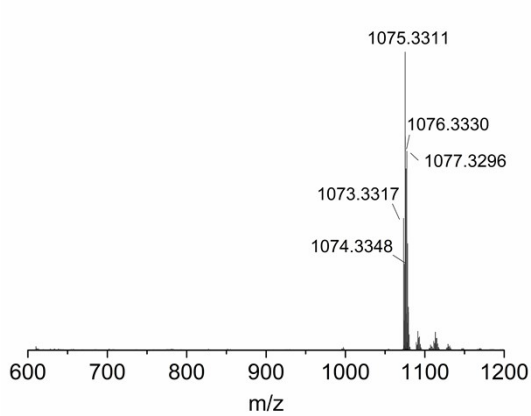

Figure S26 HRMS of compound **1b**.

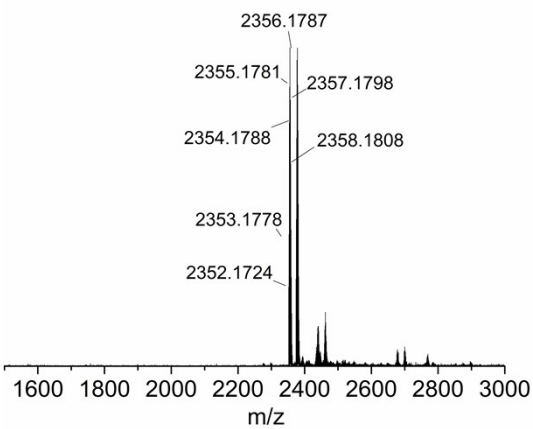

Figure S27 HRMS of compound **2a**.

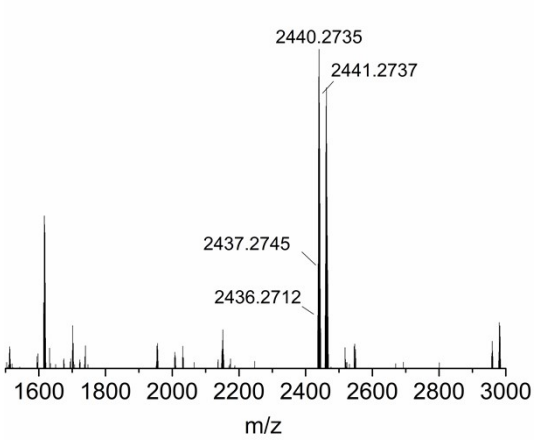

Figure S28 HRMS of compound **2b**.

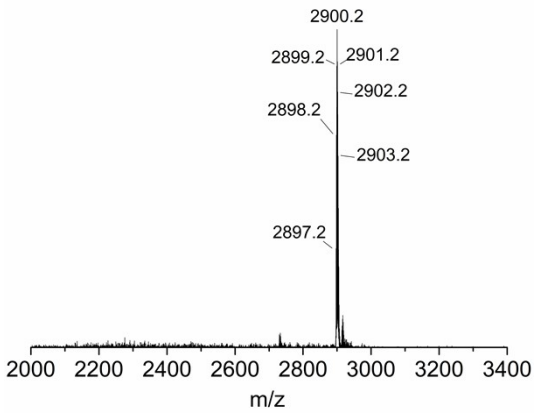

Figure S29 MALDI-TOF MS of compound **3a**.

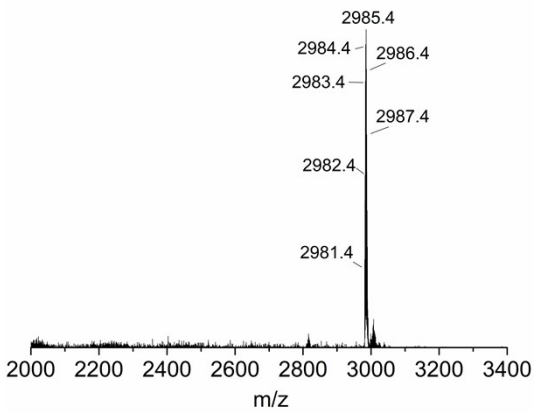

Figure S30 MALDI-TOF MS of compound **3b**.

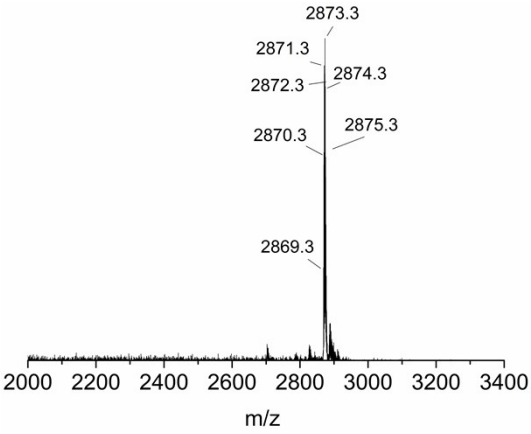

Figure S31 MALDI-TOF MS of **XW85**.

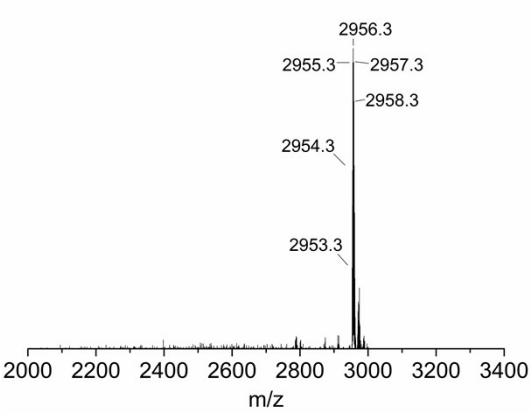

Figure S32 MALDI-TOF MS of **XW86**.

10 References

1. J. J. P. Stewart, *J. Mol. Model.*, 2007, **13**, 1173-1213.
2. M. Korth, M. Pitoňák, J. Řezáč and P. Hobza, *J. Chem. Theory Comput.*, 2010, **6**, 344-352.
3. M. Pazoki, U. B. Cappel, E. M. J. Johansson, A. Hagfeldt and G. Boschloo, *Energy Environ. Sci.*, 2017, **10**, 672-709.
4. F. Fabregat-Santiago, G. Garcia-Belmonte, I. Mora-Seró and J. Bisquert, *Phys. Chem. Chem. Phys.*, 2011, **13**, 9083-9118.